JOURNAL OF AIRCRAFT
Vol. 32, No. 1, January–February 1995

Tracking of Raindrops in Flow over an Airfoil

James R. Valentine* and Rand A. Decker†
University of Utah, Salt Lake City, Utah 84112

The splashback that occurs when raindrops impact an airfoil results in an "ejecta fog" of small droplets near the leading edge. Acceleration of these droplets by the air flowfield is a momentum sink for the airflow and has been hypothesized to contribute to the degradation of airfoil performance in heavy rain. Presented here is a one-way coupled Lagrangian particle tracking scheme to evaluate droplet concentrations and the associated momentum sink around a NACA 64-210 airfoil section for three rainfall rates. A laminar air flowfield is determined with a standard CFD code and is used as input to the particle tracking algorithm. Raindrops are assumed to be noninteracting, nondeforming, nonevaporating, and nonspinning spheres, and are tracked through the same curvilinear grid used by the airflow code. A simple model is used to simulate impacts and the resulting splashback on the airfoil surface.

Nomenclature

A_j	=	normal vector to particle entrance area j
C_D	=	particle drag coefficient
c	=	airfoil chord length
D_p	=	raindrop diameter
$D_{p,i}$	=	average raindrop diameter for interval $\Delta D_{p,i}$
$D(V - V_p)$	=	dimensionless particle drag term
g	=	gravity vector
J	=	Jacobian of the transformation between the curvilinear and Cartesian coordinate systems
$\dot{N}_{p,ij}$	=	raindrop number flow rate associated with a tracked particle
N_0	=	raindrop diameter distribution equation parameter
$N(\Delta D_{p,i})$	=	number density of raindrops having diameters in interval $\Delta D_{p,i}$
R	=	rainfall rate in mm/h
Re_p	=	particle Reynolds number
r_p	=	particle radius
S	=	dimensionless drag force acting on all droplets in a unit volume of air
t	=	dimensionless time
V	=	dimensionless local air velocity, (u, v, w)
V_{cell}	=	dimensionless volume of a computational cell
V_p	=	dimensionless particle velocity, (u_p, v_p, w_p)
V_∞	=	freestream air velocity
β	=	particle incidence angle relative to airfoil surface
Δt	=	dimensionless time step for particle motion
$\Delta t_{p,ij}$	=	dimensionless residence time of a tracked particle in a computational cell
θ	=	angular range of splashback
Λ	=	raindrop diameter distribution equation parameter
μ	=	dynamic viscosity of air
ξ	=	curvilinear coordinate position, (ξ, η, ζ)
ξ_p	=	particle position in curvilinear coordinate system, (ξ_p, η_p, ζ_p)
ξ_x, ξ_y, ξ_z	=	vectors of the metrics
ρ	=	air density
ρ_p	=	particle material density

Subscripts

i	=	raindrop diameter interval
j	=	particle entry location
p	=	particle property
$x, y, z, \xi, \eta, \zeta$	=	partial differentiation with respect to the subscripted variable

Superscript

n	=	time level

Introduction

EXPERIMENTAL data has indicated that an airfoil in heavy rain may be subject to a decrease in lift, an increase in drag, and earlier onset of stall. Several possible contributing mechanisms have been identified, including the effective "roughening" of the airfoil surface due to the presence of an uneven water film, the loss of airfoil momentum due to collisions with raindrops, and the loss of boundary-layer air momentum through the acceleration of splashed-back droplets. This article describes a numerical model to quantify the latter phenomenon. As raindrops impact an airfoil, some fraction of the incident mass is splashed back to form a droplet ejecta fog near the leading edge, while the remainder forms a thin water film on the airfoil surface, as shown in Fig. 1. It has been hypothesized that the acceleration of the splashed-back droplets by the air flowfield acts as a momentum sink, de-energizing the boundary layer and leaving it more susceptible to separation. By evaluating the momentum loss due to splashed-back droplets, modifications to the air flowfield and the resulting change in airfoil performance can be evaluated. Such research has important implications for aviation safety since several microburst-related aviation accidents in recent years have occurred during very heavy rainfall. The degradation of airfoil performance in rain is most pronounced in the high-lift configurations used in takeoffs and landings when microbursts are generally encountered and when the consequences can be most serious.

The earliest study of an aerodynamic flow in rain was performed by Rhode[2] in 1941, and indicated that the loss of aircraft momentum due to collisions with raindrops could cause

Presented as Paper 93-0168 at the AIAA 31st Aerospace Sciences Meeting and Exhibit, Reno, NV, Jan. 11–14, 1993; received March 31, 1993; revision received March 15, 1994; accepted for publication March 29, 1994.

*Graduate Student, Department of Mechanical Engineering. Student Member AIAA.

†Assistant Professor, Department of Civil Engineering. Member AIAA.

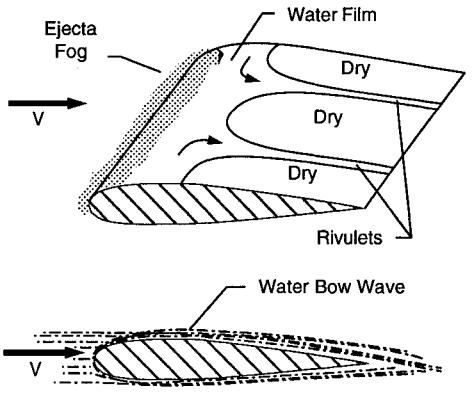

Fig. 1 Airfoil in rain showing the droplet ejecta fog and water surface film.[1]

a significant decrease in airspeed in a sufficiently heavy rainfall, but would not present a safety hazard to an aircraft cruising at an altitude of 5000 ft. In 1982, reports by Haines and Luers[3,4] analyzed the consequence of the effective roughening of the aircraft surface due to the presence of a uneven water film, and determined that this could have a larger influence on aircraft behavior than the mechanism studied previously by Rhode. Assessments of lift and drag penalties due to this effect were made for various rainfall rates. For rainfall rates as low as 100 mm/h, which are not uncommon, it was estimated that drag could increase by 5–10%, lift decrease by 10%, and decrease the stall angle of attack. In heavier rainfalls, these penalties increased. For a rainfall rate of 2000 mm/h, a decrease in lift of up to 30%, an increase in drag of up to 25%, and decrease in stall angle of attack of up to 6 deg were estimated.

During the last 10 yr, small- and large-scale experimental work has been conducted at NASA Langley Research Center with NACA 64-210, NACA 0012, and NACA 23015 airfoils.[1,5–8] Results of these tests have indicated that an airfoil in heavy rain may experience a decrease in maximum lift, an increase in drag, and earlier onset of stall. In these investigations, the boundary layer was tripped to turbulence near the leading edge of the airfoil, and the performance penalty appeared to be the result of premature separation. The effects were generally more pronounced in heavier rainfalls and in high-lift configurations with flaps and slats deployed. In other wind-tunnel experiments, laminar flow airfoils have been found to experience a performance degradation approximately equivalent to that caused by tripping the boundary layer to turbulence.[9–11]

Two approaches are commonly used to model fluid-particle flows. These models have been reviewed by Decker and Schafer[12] and Durst et al.,[13] among others. The "two fluid" or Eulerian model treats both the particle and fluid phases as continuous and solves the appropriate conservation equations for each flow. Interphase exchanges of mass, momentum, and energy are included as source terms in the appropriate conservation equations. This model is most easily implemented when particles are of a uniform size.

The "tracking" or Lagrangian approach involves solving a set of Eulerian conservation equations for the continuous fluid phase, then using Lagrangian equations of motion to determine particle trajectories. A one-way coupled model assumes that the particle motion is influenced by the fluid phase, but the fluid is unaffected by the presence of the particles. A two-way coupled model accounts for the two-way exchange of momentum (and mass and energy if applicable) between the particle and fluid phases. To account for the influence of particles on the fluid phase, source terms are added to the fluid conservation equations. Two approaches have been used in Lagrangian two-way coupled models: 1) a noniterative transient scheme where the evolution of the particle and fluid flowfields are considered simultaneously,[14] and the iterative particle-source-in-cell method,[15] where the fluid and particle fields are considered separately and updated iteratively until a stationary solution is reached.

Calarese and Hankey[16] used the two-way coupled Eulerian approach to investigate the effect of rain on the performance of a NACA 0012 airfoil for the two limiting cases of very fine (small drops) and very coarse (large drops) rain. For the case of very fine rain, increases in lift and drag were predicted as a consequence of the effective increase in fluid density, while no appreciable change in airfoil performance was observed for coarse rain, which is contrary to experimental results. However, this analysis neglected the effects of splashed-back droplets and the rough water surface film, indicating the importance of these mechanisms.

The present study uses the one-way coupled Lagrangian approach to determine splashed-back droplet concentrations and the associated airflow momentum sink around a NACA 64-210 airfoil. The incompressible, laminar air flowfield is determined with an existing thin layer Navier-Stokes code,[17] and Lagrangian equations of motion are used to track nonevaporating, noncolliding, nondeforming, and nonspinning spherical particles through the air flowfield. Raindrop impacts on the airfoil surface and the resulting breakup and reinjection of droplets into the flow are modeled in the particle tracking code.

The assumption of noninteracting droplets is justified by Bilanin's[18] observation that even at an extremely high rainfall of 1872 mm/h and for an average raindrop diameter of 4 mm, the mean distance between raindrops will be of the order of 7 cm, or 17.5 times the drop diameter. Thus, raindrop collisions should occur infrequently enough to be negligible. Bilanin[18] has also analyzed the effect of evaporation of droplets near the airfoil surface and concluded that this should not degrade the lift characteristics of an airfoil. The assumption of nondeforming, spherical droplets simplifies the analysis, but in reality raindrops will deform as they enter the airfoil boundary layer. There may also be some breakup of raindrops in the boundary layer if a critical Weber number is reached.[19]

Numerical Algorithm

Air Flowfield Determination

The air flowfield is determined with FMC1, a three-dimensional flux-difference splitting code for the thin-layer approximation of the Navier-Stokes equations, the details of which have been reported previously[17] and will not be repeated here. The code and boundary conditions have been adapted to simulate two-dimensional flow over an airfoil as described below.

The computational domain consists of an O-H grid around a NACA 64-210 airfoil section, a spanwise cross section of which is shown in Fig. 2. Grid dimensions are 65 normal to the surface (ξ), by 3 spanwise (η), by 163 circumferential (ζ), although there is no variation of the flowfield in the spanwise direction. Boundary conditions are no-slip and zero normal pressure gradient at the airfoil surface. Properties are averaged at the branch cut ($\zeta = 1$ and $\zeta = 163$) in the wake. The laminar air flowfield is determined for an angle of attack of 4.039 deg, and a Reynolds number of $Re = 2.6 \times 10^6$. The airfoil chord length is set to 1 m, in which case the freestream air velocity becomes $V_\infty \approx 38$ m/s. This air flowfield is input to the particle tracking algorithm.

Particle Tracking Algorithm

Assuming that particles are subject only to drag and gravity forces, the dimensionless equation of particle motion can be written as

$$\frac{dV_p}{dt} = D(V - V_p) \times (V - V_p) + \frac{c}{V_\infty^2} g \qquad (1)$$

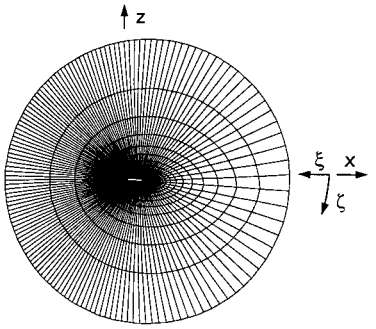

Fig. 2 Spanwise cut of the 65 × 3 × 163 computational grid.

where velocities have been nondimensionalized by V_∞, lengths by c, and time by c/V_∞. The dimensionless drag term in Eq. (1) is

$$D(V - V_p) = \frac{3\rho c C_D |V - V_p|}{8 r_p \rho_p} \tag{2}$$

where the drag coefficient for a spherical particle can be represented by

$$C_D = \max[0.44, (24/Re_p)(1 + 0.15 Re_p^{0.687})] \tag{3}$$

The second term in the brackets is as suggested by Wallis[20] for particle Reynolds numbers to 10^3, and the first term extends the validity of the expression. The particle Reynolds number is defined in terms of the dimensionless velocities V and V_p as

$$Re_p = [\rho |V_x(V - V_p)| 2 r_p/\mu] \tag{4}$$

Maximum Reynolds number of the splashed-back droplets are of the order of 1.5×10^4.

A second particle trajectory equation is the chain rule expression

$$\frac{d\boldsymbol{\xi}_p}{dt} = \boldsymbol{\xi}_x u_p + \boldsymbol{\xi}_y v_p + \boldsymbol{\xi}_z w_p \tag{5}$$

where $\boldsymbol{V}_p = (u_p, v_p, z_p)$ represents Cartesian components of the particle velocity. The metric terms in Eq. (5) are defined as

$$\begin{aligned} \boldsymbol{\xi}_x &= (\xi_x, \eta_x, \zeta_x) \\ \boldsymbol{\xi}_y &= (\xi_y, \eta_y, \zeta_y) \\ \boldsymbol{\xi}_z &= (\xi_z, \eta_z, \zeta_z) \end{aligned} \tag{6}$$

and are evaluated at the particle position through linear interpolation of the values at gridpoints. At each gridpoint, metrics are evaluated by the expressions[21]

$$\begin{aligned} \xi_x &= J(y_\eta z_\zeta - y_\zeta z_\eta) \\ \xi_y &= -J(x_\eta z_\zeta - z_\xi z_\eta) \\ \xi_z &= J(x_\eta y_\zeta - x_\zeta y_\eta) \\ \eta_x &= -J(y_\xi z_\zeta - y_\zeta z_\xi) \\ \eta_y &= J(x_\xi z_\zeta - x_\zeta z_\xi) \\ \eta_z &= -J(x_\xi y_\zeta - x_\zeta y_\xi) \\ \zeta_x &= J(y_\xi z_\eta - y_\eta z_\xi) \\ \zeta_y &= -J(x_\xi z_\eta - x_\eta z_\xi) \\ \zeta_z &= J(x_\xi y_\eta - x_\eta y_\xi) \end{aligned} \tag{7}$$

and the Jacobian by

$$J^{-1} = x_\xi(y_\eta z_\zeta - y_\zeta z_\eta) - x_\eta(y_\xi z_\zeta - y_\zeta z_\xi) + x_\zeta(y_\xi z_\eta - y_\eta z_\xi) \tag{8}$$

where subscripts indicate partial differentiation. The partial derivatives x_ξ, x_η, x_ζ, y_ξ, etc., are approximated with second-order-accurate finite differences.

In three-dimensional space, Eqs. (1) and (5) form a set of six ordinary differntial equations that can be integrated numerically by any one of a number of standard schemes (i.e., Euler's method, Runge-Kutta, etc.). However, following the example of Crowe et al.,[15] Eq. (1) is approximately integrated analytically. By assuming the particle Reynolds number and air velocity to be constant over one time step of particle travel, the integration of Eq. (1) yields

$$\begin{aligned} V_p^{n+1} = {} & V^n - (V^n - V_p^n) e^{(-D^n \Delta t)} \\ & + g\{c[1 - e^{(-D^n \Delta t)}]/V_\infty^2 D^n\} \end{aligned} \tag{9}$$

where $D^n = D(V^n - V_p^n)$, as in Eq. (2). This analytical integration of Eq. (1) improves computational efficiency, and was also found to reduce numerical stability problems in the determination of trajectories of very small particles.

Equation (5) is integrated with a modified Euler scheme. Using metrics evaluated at the current particle position, the contravariant velocity $d\xi/dt$ is calculated at the current time level n as

$$\left.\frac{d\boldsymbol{\xi}_p}{dt}\right|^n = \boldsymbol{\xi}_x^n u_p^n + \boldsymbol{\xi}_y^n v_p^n + \boldsymbol{\xi}_z^n w_p^n \tag{10}$$

then this velocity is used to predict the particle's next position

$$\boldsymbol{\xi}_p^* = \boldsymbol{\xi}_p^n + \left.\frac{d\boldsymbol{\xi}_p}{dt}\right|^n \Delta t \tag{11}$$

The local metrics are calculated at this predicted position and are used with particle velocities from Eq. (9) to determine a new contravariant velocity

$$\left.\frac{d\boldsymbol{\xi}_p}{dt}\right|^* = \boldsymbol{\xi}_x^* u_p^{n+1} + \boldsymbol{\xi}_y^* v_p^{n+1} + \boldsymbol{\xi}_z^* w_p^{n+1} \tag{12}$$

The particle position is advanced using the average of the two contravariant velocities from Eqs. (10) and (12):

$$\boldsymbol{\xi}_p^{n+1} = \boldsymbol{\xi}_p^n + \frac{1}{2}\left(\left.\frac{d\boldsymbol{\xi}_p}{dt}\right|^n + \left.\frac{d\boldsymbol{\xi}_p}{dt}\right|^*\right) \Delta t \tag{13}$$

At each position a time step is calculated based on a particle residence time of four steps in the current cell.

Modeling of Rain

Ground level rainfall rates are generally measured in terms of millimeters or inches of water accumulation per hour. The heaviest ever recorded 1 min duration ground level rainfall measured 1874 mm/h,[22] but typically rates are much lower than this, with the heaviest rainfalls occurring for short periods of 30 s or less. Dunham[6] has estimated that at any location in the subtropical maritime southeastern U.S., a total of approximately 2 min of 200 mm/h or heavier rainfall can be expected during the span of 1 yr.

During a thunderstorm, significantly higher rain intensities than those at ground level can be expected at a higher altitude. The rain measurement parameter used above ground level is liquid water content (LWC), or the mass of water per unit volume of air. LWC is also important in wind-tunnel testing,

since the actual rainstorm value must be conserved in small-scale experiments.[18] Roys and Kessler[23] have taken airborne measurements of LWC within several Great Plains thunderstorms, and reported an average value of 8.7 g/m^3 and a peak value of 44 g/m^3.

The drop-size distribution of ground level rain can be approximated by the expression[24]

$$N(D_p) = N_0 \exp(-\Lambda D_p) \tag{14}$$

where $N(D_p)$ is the number of raindrops of diameter D_p (in mm) per cubic meter of air. For thunderstorm rain, values of $N_0 = 1.4 \times 10^3$ m^{-3}mm^{-1} and $\Lambda = 3.0 \times R^{-0.21}$ have been determined.[25] Multiplying the raindrop diameter distribution given by Eq. (14) by the mass of the raindrop, then integrating over the range of drop diameters, results in an expression that relates ground level rainfall rates and LWC. Assuming a raindrop diameter range from 0 to 6 mm, the average value of LWC of 8.7 g/m^3 measured by Roys and Kessler[23] corresponds to a ground level rainfall rate of 424 mm/h.

For modeling purposes, the continuous distribution of raindrop diameters is divided into four discrete intervals, $\Delta D_{p,i}$ for $i = 1$–4. The number density of raindrops in each interval is given by

$$N(\Delta D_{p,i}) = \int_{\Delta D_{p,i}} N_0 \exp(-\Lambda D_p)\, dD_p \tag{15}$$

and the average diameter of raindrops in the interval by

$$D_{p,i} = \frac{\int_{\Delta D_{p,i}} D_p N_0 \exp(-\Lambda D_p)\, dD_p}{N(\Delta D_{p,i})} \tag{16}$$

Both of these integrals are easily evaluated. The four diameter intervals used in this study are $0 < D_p < 1$ mm for $\Delta D_{p,1}$, 1 mm $< D_p < 2$ mm for $\Delta D_{p,2}$, 2 mm $< D_p < 3$ mm for $\Delta D_{p,3}$, and 3 mm $< D_p < 6$ mm for $\Delta D_{p,4}$.

Particles enter the computational domain from discrete locations with an initial horizontal velocity of V_∞, and an initial vertical velocity determined by equating the gravity and vertical drag forces. Ideally, the entry locations should be placed at the outer grid boundary, but some reduction of computational effort is realized if the particles are tracked only in the vicinity of the airfoil where velocity gradients that may alter the particle trajectories are present. Thus, particles are tracked only within the region inside the fifth circumferential gridline ($\xi = 5$) from the outer edge of the computational domain, an area of approximately two chord lengths in all directions from the airfoil surface. Each entry location j has an associated area A_j through which raindrops enter, and so the raindrop number flow rate from j and for diameter interval $\Delta D_{p,i}$ can be expressed as

$$\dot{N}_{p,ij} = N(\Delta D_{p,i})(V_{p\infty,i} \cdot A_j) \tag{17}$$

where $N(\Delta D_{p,i})$ is the raindrop number density from Eq. (15), and $(V_{p\infty,i} \cdot A_j)$ is the dot product of the dimensionless free-stream velocity of particles of $D_{p,i}$ and A_j. Thus, for each drop-size interval $\Delta D_{p,i}$, and each j, one particle is tracked through the domain and is associated with $\dot{N}_{p,ij}$. $D_{p,i}$ from Eq. (16) is used as the tracked particle diameter. Approximately 44,000 entry locations are used.

Impact Model

Feo[26] has reported on the characteristics of high incidence water drop impacts such as those that occur near the leading edge of an airfoil in rain. His measurements were for 4-mm-diam water drops at an incident velocity of 60 m/s. Under these conditions, approximately 20% of the incident drop was splashed back while the remainder stayed on the impacted surface. At the beginning of the splash process, droplets having diameters of the order of a few microns were splashed back at a velocity of approximately seven times that of the incident drop in a hollow cone-shaped pattern over an angular range of about 100 deg. As the splash progressed in time, the diameters of the splashed-back droplets increased by an order of magnitude, the velocities decreased to approximately the incident velocity, and the angular range of splashback increased to about 170 deg. Approximately half of splashback occurred during the later stages of the splash process when the ejected droplets had a velocity of, at most, twice the incident velocity. For similar incident drop conditions, Bilanin[19] has used conservation laws to analytically estimate the diameter of splashed-back droplets as being of the order of magnitude of 1–100 μm.

The two-dimensional splash model used in the particle tracking code is based on Feo's observations and is shown in Fig. 3. The characteristics of splashed-back droplets are taken as approximately average values for the duration of an actual splash. It is assumed that 20% of the mass of the incident drop is reinjected as droplets of diam 20 μm over an angular range that varies from $\theta = 180$ deg for a perpendicular impact ($\beta = 90$ deg) to $\theta = 0$ deg for a tangential impact ($\beta = 0$ deg). The angular range of reinjection is centered around a reinjection angle equal to the incident angle, and the velocity of the reinjected droplets is assumed equal to three times the velocity of incident drop. Actual particle impacts as determined by this model are shown in Fig. 4.

Particle Field Statistics

Particle field statistics are collected in cells bounded by gridlines, then averaged over neighboring cells to determine the values at gridpoints. Steady-state particle concentrations are calculated by tabulating the residence time of each particle in each cell, and particle drag distributions by tabulating the total drag acting on each particle during its residence time in each cell. These quantities are modified according to $\dot{N}_{p,ij}$.

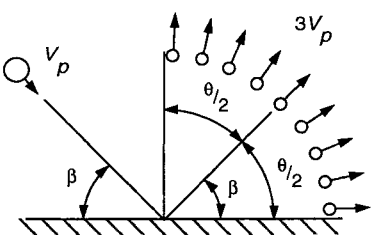

Fig. 3 Two-dimensional impact model. The angular range of reinjection (θ) varies linearly from 180 deg for a perpendicular impact ($\beta = 90$ deg) to 0 deg for a tangential impact ($\beta = 0$ deg).

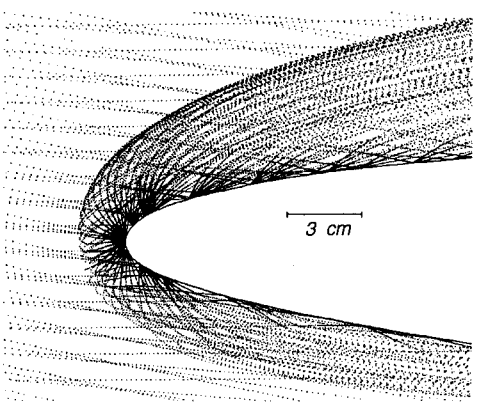

Fig. 4 Droplet trajectories and impacts at the leading edge of the airfoil. Approximate 3 cm/scale assumes an airfoil chord length of 1 m.

Dimensionless particle drag distributions are collected on a per volume basis for each grid cell as

$$S = \frac{1}{V_{\text{cell}}} \sum_{i,j} \left[\frac{1}{2} \pi \frac{r_p^2}{c^2} C_D |V - V_p| (V - V_p) \right] \dot{N}_{p,ij} \Delta t_{p,ij} \quad (18)$$

where velocities are averaged over the time step, V_{cell} is the dimensionless volume of the cell (scaled by the cube of the airfoil chord length), the particle drag coefficient C_D is determined with Eq. (3) and averaged over the time step, $\dot{N}_{p,ij}$ is the raindrop number flow rate from Eq. (17) associated with the particle, and $\Delta t_{p,ij}$ is the residence time of the particle in the cell. The bracketed term in Eq. (18) represents the dimensionless drag force acting on a particle, and the sum is over all particles that traverse the cell for all diameter intervals i and all particle entry locations j. The vector quantity S determined in Eq. (18) is nondimensionalized in the same manner as the Navier-Stokes equations, and so it represents the momentum source/sink experienced by the air flowfield due to particle drag, and should be included in the Navier-Stokes equations to account for the particle effect on fluid motion. If components of S are positive, they represent a momentum sink for the airflow and act to decrease the momentum of the boundary layer.

Results

Figure 5 shows droplet concentrations around the airfoil for R = 100, 300, and 500 mm/h. Since the freestream raindrop number density is of the order of 10^3 raindrops/m^3, and well below the value of the first contour level, it can be assumed that the vast majority of droplets near the airfoil are due to splashback. The formation of a high-concentration region similar to the ejecta fog and water bow wave shown in Fig. 1 can be seen. For a chord length of 1 m, the thickness of this layer varies from approximately 2 cm at the leading edge of the airfoil to approximately 10 cm further downstream along the upper surface. The layer is more dense on the upper surface of the airfoil and also for higher rainfall rates. For an angle of attack of 4.039 deg, the stagnation point is slightly below the leading edge, thus, splashed-back droplets from raindrop impacts at the leading edge tend to be carried over the upper surface of the airfoil more than the lower surface. In addition, the downward component of raindrop velocity results in more impacts on the upper surface, especially for larger raindrops that have higher vertical velocities.

The magnitude of the dimensionless particle drag [$|\underline{S}|$ from Eq. (18)] is plotted in Figs. 6 and 7. When this term becomes sufficiently large, the boundary layer may lose momentum,

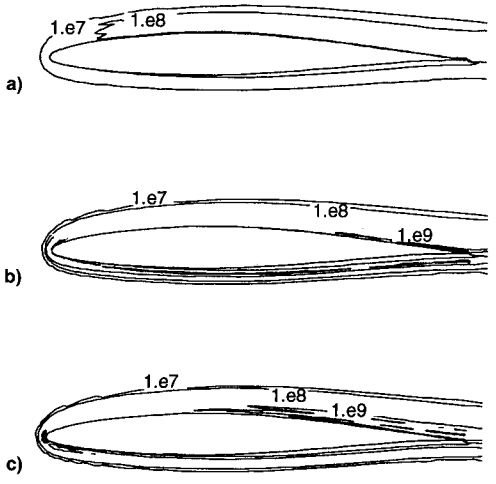

Fig. 5 Splashed-back droplet concentrations (droplets/m^3) around the airfoil for three rainfall rates. R = a) 100 mm/h, maximum = 1.2e9; b) 300 mm/h, maximum 3.6e9; and c) 500 mm/h, maximum = 5.1e9.

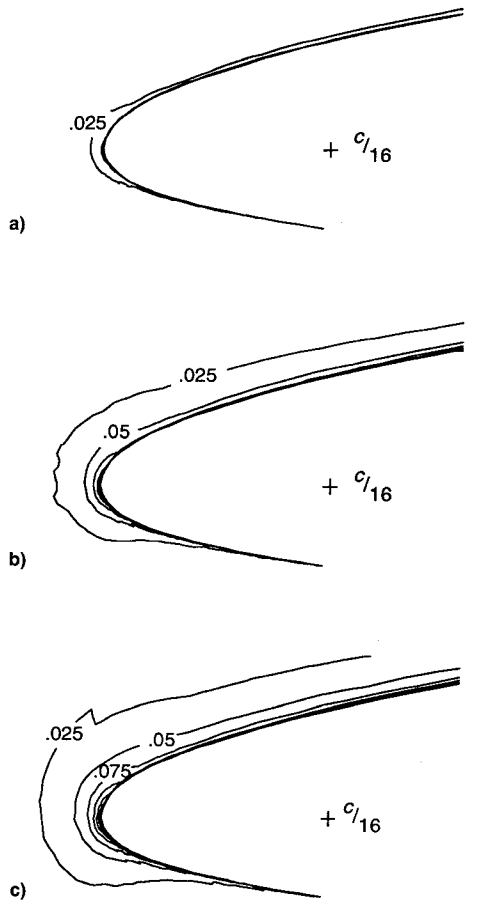

Fig. 6 Magnitude of the airflow momentum source/sink due to particle drag [$|S|$ from Eq. (18)] at the leading edge of the airfoil for three rainfall rates. R = a) 100 mm/h, maximum = 0.085; b) 300 mm/h, maximum = 0.189; and c) 500 mm/h, maximum = 0.267. One-sixteenth chord position marked for reference.

Fig. 7 Extent of the air flow momentum source/sink due to particle drag [$|S|$ from Eq. (18)] for a rainfall rate of R = 500 mm/h, maximum = 0.267. One-half chord position marked for reference.

resulting in decreased lift and a possible premature separation and stall. For R = 100 mm/h, the region of momentum loss is confined to a small area near the leading edge of the airfoil. As the rainfall rate increases, however, the extent of this region grows and the maximum value, which occurs at the leading edge, increases. For R = 500 mm/h, the region extends to approximately the one-half chord position, and a maximum value of 0.267 is obtained at the leading edge of the airfoil. Assuming that the dominant terms of the nondimensionalized Navier-Stokes equations are of the order of magnitude of 1, a term with a value of 0.267 may have a significant contribution. Thus, the drag of splashed-back droplets may have the potential of altering the boundary-layer flow.

Concluding Remarks

A particle tracking scheme has been coupled with a thin layer Navier-Stokes code to model the flow of rain over an airfoil and the splashback of droplets from raindrop impacts on the airfoil surface. Numerical results show a region of high droplet concentration corresponding to the ejecta fog and water bow wave observed experimentally. The drag of splashed-back droplets acts as a momentum sink near the leading edge

of the airfoil, and has the potential to de-energize the boundary layer and contribute to a degradation of airfoil performance in rain. It should be kept in mind that a rain-induced airfoil performance penalty is not due to this effect alone; the effective roughening of the airfoil surface due to an uneven water film may also be a contributor.

Further experimental analysis is needed to verify the accuracy of the numerical scheme. A simple splashback model is used to represent a complex, time-dependent process, and a question arises of whether it adequately captures the physics of an actual splash. Variations in the fraction of raindrop mass splashed back and the initial velocities, diameters, and directions of the splashed-back droplets all have the potential to alter the results presented here. The characteristics of the splashback may be functions of the incident raindrop velocity and diameter, the angle of incidence, and the thickness of the water surface film. At this point, the splashback model is based entirely on data for one set of incident drop conditions, thus, further experimental observations of the splash process must be made.

Raindrops are assumed to be nondeforming spheres and deformation to a nonspherical shape will change their drag characteristics. Although this may not be important for the incident raindrops, it could be more critical for the splashed-back droplets since their drag can alter the boundary-layer flow. This may require some compensation in the splashback model. Raindrops may also break up as they enter the airfoil boundary layer if a critical Weber number is reached, altering the diameter distribution that strikes the airfoil surface, which in turn could change the characteristics of the splashed-back droplets.

These results establish a basis for determining one part of the airfoil performance penalty associated with heavy rain. The present analysis is the first step in developing a fully two-way coupled simulation where the air flowfield is recalculated, this time accounting for momentum loss due to particle drag. Thus, the effect of the drag of splashed-back particles on airfoil performance can be quantitatively analyzed, and lift and drag predictions can be compared to wind-tunnel data.[1] A more comprehensive scheme may aso require the inclusion of the effect of the rough water surface film on airfoil performance.

Acknowledgments

The authors wish to acknowledge the support (NASA Contract NAG-1-1232) of the Heavy Rain Research Group in the Subsonic Aerodynamics Branch, Applied Aerodynamics Division, NASA Langley Research Center, Hampton, Virginia.

References

[1]Bezos, G. M., Dunham, R. E., Jr., Gentry, G. L., Jr., and Melson, W. E., Jr., "Wind Tunnel Aerodynamic Characteristics of a Transport-Type Airfoil in a Simulated Heavy Rain Environment," NASA TP-3184, Aug. 1992.

[2]Rhode, R. V., "Some Effects of Rainfall on Flight of Airplanes and on Instrument Indications," NACA TN 803, April 1941.

[3]Haines, P. A., and Luers, J. K., "Aerodynamic Penalties of Heavy Rain on Landing Aircraft," *Journal of Aircraft*, Vol. 20, No. 2, 1983, pp. 111–119.

[4]Luers, J. K., and Haines, P. A., "Heavy Rain Influence on Airplane Accidents," *Journal of Aircraft*, Vol. 20, No. 2, 1983, pp. 187–191.

[5]Bezos, G. M., Dunham, R. E., Jr., Gentry, G. L., Jr., and Melson, W. E., Jr., "Wind Tunnel Test Results of Heavy Rain Effects on Airfoil Performance," AIAA Paper 87-0260, Jan. 1987.

[6]Dunham, R. E., Jr., "The Potential Influence of Rain on Airfoil Performance," *Influence of Environmental Factors on Aircraft Wing Performance*, von Kármán Inst. for Fluid Dynamics, Rhode-Saint-Genese, Belgium, Feb. 1987.

[7]Campbell, B. A., and Bezos, G. M., "Steady State and Transitional Aerodynamic Characteristics of a Wing in Simulated Heavy Rain," NASA TP-2932, Aug. 1989.

[8]Bezos, G. M., Campbell, B. A., and Melson, W. E., Jr., "The Development of a Capability for Aerodynamic Testing of Large-Scale Wing Sections in a Simulated Natural Rain Environment," AIAA Paper 89-0762, Jan. 1989.

[9]Yip, L. P., "Wind Tunnel Investigation of a Full-Scale Canard-Configured General Aviation Aircraft," NASA TP-2382, March 1985.

[10]Hansman, R. J., Jr., and Barsotti, M. F., "Surface Wetting Effects on a Laminar Flow Airfoil in Simulated Heavy Rain," *Journal of Aircraft*, Vol. 22, No. 12, 1985, pp. 1049–1053.

[11]Hansman, R. J., Jr., and Craig, A. P., "Low Reynolds Number Tests of NACA 64-210, NACA 0012, and Wortmann FS67-K170 Airfoils in Rain," *Journal of Aircraft*, Vol. 24, No. 8, 1987, pp. 559–566.

[12]Decker, R., and Schafer, C. F. (eds.), "Mixing and Demixing Processes in Multiphase Flows with Application to Propulsion Systems," NASA CP-3006, Feb. 1988.

[13]Durst, F., Milojevic, D., and Schönung, B., "Eulerian and Lagrangian Predictions of Particulate Two-Phase Flows: A Numerical Study," *Applied Mathematical Modelling*, Vol. 8, April 1984, pp. 101–115.

[14]Dukowicz, J. K., "A Particle-Fluid Numerical Model for Liquid Sprays," *Journal of Computational Physics*, Vol. 35, No. 2, 1980, pp. 229–253.

[15]Crowe, C. T., Sharma, M. D., and Stock, D. E., "The Particle-Source-in-Cell (PSI-Cell) Model for Gas-Droplet Flows," *Journal of Fluids Engineering*, Vol. 99, June 1977, pp. 325–332.

[16]Calarese, W., and Hankey, W. L., "Numerical Analysis of Rain Effects on an Airfoil," AIAA Paper 84-0539, Jan. 1984.

[17]Hartwich, P.-M., and Hsu, C.-H., "High Resolution Upwind Schemes for the Three-Dimensional Navier-Stokes Equations," *AIAA Journal*, Vol. 26, No. 11, 1988, pp. 1321–1328.

[18]Bilanin, A. J., "Scaling Laws for Testing Airfoils Under Heavy Rainfall," *Journal of Aircraft*, Vol. 24, No. 1, 1987, pp. 31–37.

[19]Wierzba, A., "Deformation and Breakup of Liquid Drops in a Gas Stream at Nearly Critical Weber Numbers," *Experiments in Fluids*, Vol. 9, Nos. 1/2, 1990, pp. 59–64.

[20]Wallis, G. B., *One-Dimensional Two-Phase Flow*, McGraw-Hill, New York, 1969, p. 178.

[21]Anderson, D. A., Tannehill, J. C., and Pletcher, R. H., *Computational Fluid Mechanics and Heat Transfer*, Hemisphere, New York, 1984, pp. 252, 253.

[22]Riordan, P., "Weather Extremes Around the World," U.S. Army, TR 70-45-ES, Washington, DC, Jan. 1970.

[23]Roys, G. P., and Kessler, E., "Measurements by Aircraft of Condensed Water in Great Plains Thunderstorms," U.S. Dept. of Commerce, TN 49-NSSP-19, July 1966.

[24]Marshall, J. S., and Palmer W. McK., "The Distribution of Raindrops with Size," *Journal of Meteorology*, Vol. 5, No. 4, 1948, pp. 165, 166.

[25]Joss, J., and Waldvogel, A., "Raindrop Size Distribution and Sampling Size Errors," *Journal of the Atmospheric Sciences*, Vol. 26, No. 3, 1969, pp. 566–569.

[26]Feo, A., "Waterdrop Splashback Characteristics of a Perpendicular Impact Near an Air Stagnation Point," Instituto Nacional de Tecnologia Agropecuaria, INTA Nota Tecnica N/221/501/89.025, Madrid, Spain, Sept. 1989.